Fluorescent Probes | Hot Paper

International Edition: DOI: 10.1002/anie.201502403
German Edition: DOI: 10.1002/ange.201502403

Photoelectrocyclization as an Activation Mechanism for Organelle-Specific Live-Cell Imaging Probes**

*Mai N. Tran and David M. Chenoweth**

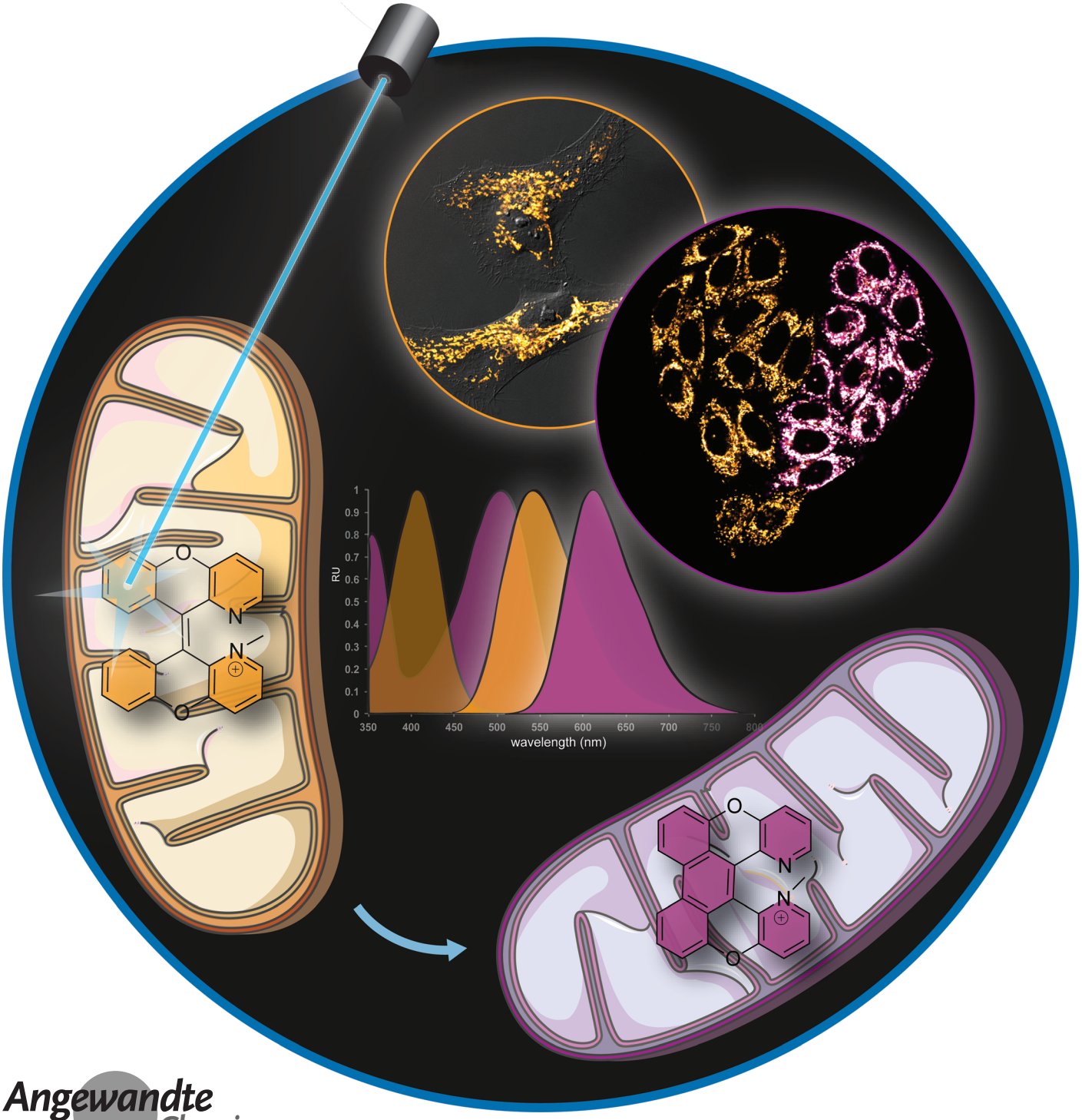

Abstract: *Photoactivatable fluorophores are useful tools in live-cell imaging owing to their potential for precise spatial and temporal control. In this report, a new photoactivatable organelle-specific live-cell imaging probe based on a 6π electrocyclization/oxidation mechanism is described. It is shown that this new probe is water-soluble, non-cytotoxic, cell-permeable, and useful for mitochondrial imaging. The probe displays large Stokes shifts in both pre-activated and activated forms, allowing simultaneous use with common dyes and fluorescent proteins. Sequential single-cell activation experiments in dense cellular environments demonstrate high spatial precision and utility in single- or multi-cell labeling experiments.*

Photoactivatable fluorescent probes are powerful tools for studying biological systems owing to the high spatial and temporal control afforded by light. Photoactivatable probes can be genetically encoded proteins[1] or small molecules.[2] Each of these technologies comes with its own benefits and limitations and may be thought of as complimentary to one another depending on the application. The protein "Kaede" represents the first discovery of a photoactivatable fluorescent protein, and much progress has been made in recent years with similar genetically encoded approaches.[3] Small-molecule photoactivatable probes have also found widespread use, and they generally rely on a small number of photoactivation mechanisms, such as photoisomerization,[4] photouncaging,[5] photodecomposition of azides,[6] or photoclick reactions.[7] These strategies primarily depend on the conversion from an initial non-fluorescent state into a fluorescent state.

Herein, we present a new intracellular imaging probe that utilizes a photoactivation mechanism based on a photochemically allowed 6π electrocyclization/oxidation reaction. This mechanism expands the toolbox for intracellular photoactivatable probes, providing an emissive pre- and post-activated form that can be tracked by fluorescence microscopy. To demonstrate this strategy, we introduce a water-soluble, non-cytotoxic, and readily cell-permeable photoactivatable fluorescent probe for mitochondrial-specific live-cell imaging. We compare the cytotoxicity of this probe to a commonly used

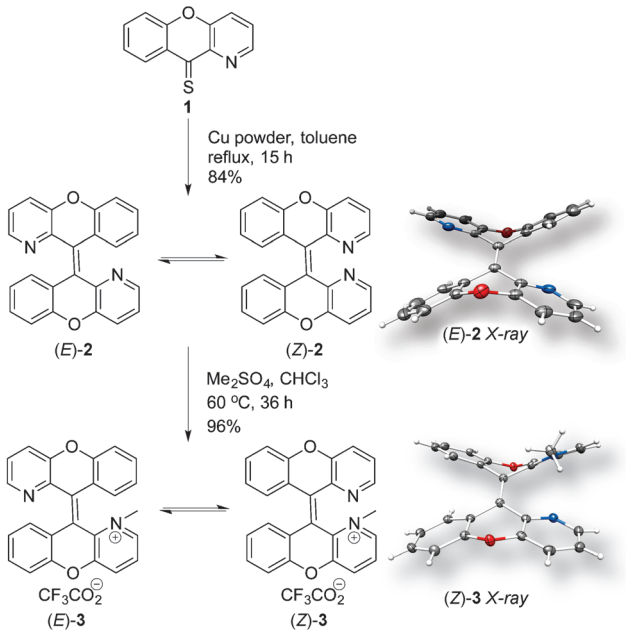

Scheme 1. Synthesis of (*E*)-**3**/(*Z*)-**3** and crystal structures of (*E*)-**2** and (*Z*)-**3**.

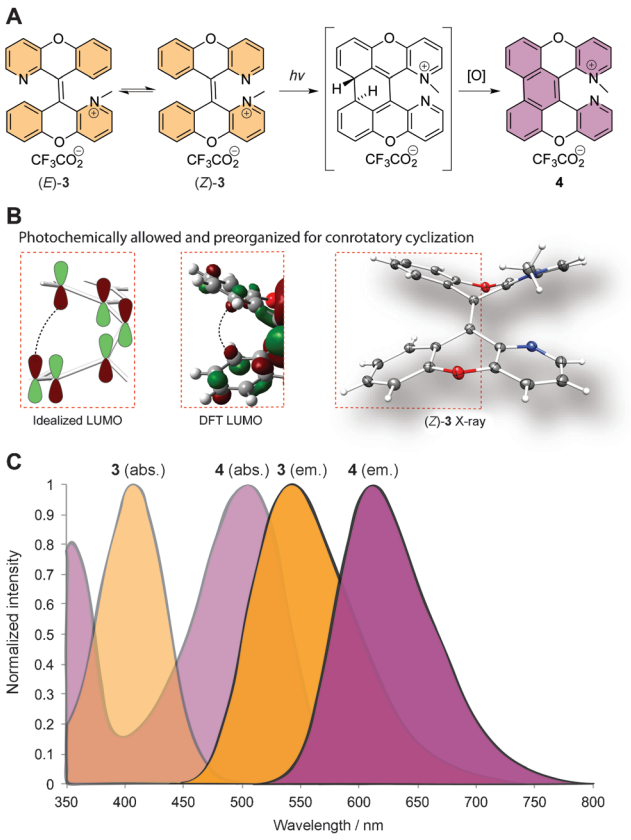

Figure 1. A) *E*–Z interconversion and photocyclization/oxidation reaction of (*E*)-**3**/(*Z*)-**3**. B) Idealized and calculated LUMO of (*Z*)-**3** (TD-DFT B3LYP, 6-311+G(2d,p) basis set). Note the orbital preorganization for photochemically favored conrotatory cyclization. C) Absorbance and emission spectra of (*E*)-**3**/(*Z*)-**3** [λ_{max} = 408 nm (abs.), 543 nm (em.), ε = 11 040 $M^{-1}cm^{-1}$, Φ_F = 0.021, τ = 0.97 ns] and **4** [λ_{max} = 504 nm (abs.), 612 nm (em.), ε = 11 496 $M^{-1}cm^{-1}$, Φ_F = 0.100, τ = 4.77 ns] in water.

[*] M. N. Tran, Prof. D. M. Chenoweth
Department of Chemistry, University of Pennsylvania
231 South 34th Street, Philadelphia, PA 19104 (USA)
E-mail: dcheno@sas.upenn.edu

[**] This work was supported by funding from the University of Pennsylvania. We thank the Vietnam Education Foundation for funding (VEF Fellowship to M.N.T.) and the NSF for support of the X-ray diffractometer (Grant CHE-0840438). We thank Dr. George Furst and Dr. Rakesh Kohli for assistance in obtaining the high-resolution NMR and mass spectral data, respectively. We are grateful to Dr. Patrick Carroll for X-ray crystallographic assistance. We thank Tom Troxler for assistance with the TCSPC measurements collected at the Ultrafast Optical Processes Laboratory at the University of Pennsylvania (supported by the NIH, Grant P41GM104605). We thank Mike Lampson and The Penn CDB Microscopy Core facility for microscope use.

Supporting information for this article is available on the WWW under http://dx.doi.org/10.1002/anie.201502403.

and commercially available mitochondrial dye.[8] We also demonstrate its utility in spatiotemporally defined live-cell imaging of mitochondria in dense cellular populations through sequential single-cell activation experiments.

First, we developed a rapid and efficient synthesis of the desired photoactivatable probe starting with commercially available 2-cyanopyridine (Supporting Information, Scheme S1). Following a similar route to that reported in our previous studies,[9] we elaborated 2-cyanopyridine to thioketone **1**. Homocoupling of **1** using copper powder in toluene at reflux yielded 1,1′-diazaxanthilidene **2** as an interconverting mixture of the *E* and *Z* isomers in 84% yield (Scheme 1). Methylation of **2** with dimethyl sulfate afforded the desired monomethylated product (*E*)-**3**/(*Z*)-**3** in 96% yield. The overall yield of the probe from the commercially available starting materials after six steps was 24% (Scheme S1, Scheme 1). Single crystals of (*E*)-**2** and (*Z*)-**3** were obtained by slow evaporation from chloroform/methanol (1:1) and water solutions, respectively. Both structures adopted an *anti*-folded conformation, despite the increased steric hindrance from methylation in (*Z*)-**3** (Scheme 1). Variable-temperature ^{1}H NMR spectroscopy[10] of (*E*)-**2**/(*Z*)-**2** in deuterated *N*,*N*-dimethylformamide confirmed the dynamic interconversion of the *E* and *Z* isomers at room temperature, which is consistent with our previous studies (Figure S2).[9] At low temperature, separate sets of sharp and well-resolved signals were observed for the *E* and *Z* isomers of **3**. Incremental heating resulted in significant signal broadening followed by sharpening and resolved coupling at high temperature. This result indicates rapid exchange on the NMR timescale. Coalescence was observed at 45 °C, and the activation energy was determined to be $\Delta G^{\ddagger} = 15.7$ kcal mol^{-1} (Figure S1).

Upon irradiation at 365 nm using a Rayonet photoreactor, the (*E*)-**3**/(*Z*)-**3** mixture was found to undergo photocyclization followed by oxidation to yield photoproduct **4** (Figure 1 A). To promote the photocyclization step of (*E*)-**3**/(*Z*)-**3**, both the *anti*-folded conformation and dynamic interconversion are crucial. According to the Woodward–Hoffmann rules, electrocyclization of the 1,3,5-hexatriene moiety of (*Z*)-**3** ($4n+2$ electron system) is thermally allowed in a disrotatory manner and photochemically allowed in a conrotatory manner.[11] The *anti*-folded conformation of (*Z*)-**3** is preorganized for conrotatory cyclization, satisfying the requirement for the photochemical reaction. This conclusion was further confirmed by TD-DFT calculations[12] on (*Z*)-**3**. As is evident from the calculated molecular orbitals, a conrotatory cyclization leads to constructive interactions and is photochemically favored (Figure 1 B). The structure of (*E*)-**3** is disfavored for electrocyclization but *E*–*Z* isomerization leads to the formation of (*Z*)-**3**, facilitating the photoreaction. As a result, the dihydrophenanthrene intermediate was attained, which was followed by oxidation to give photoproduct **4**. The dihydrophenanthrene intermediate was not isolable from the reaction mixture.

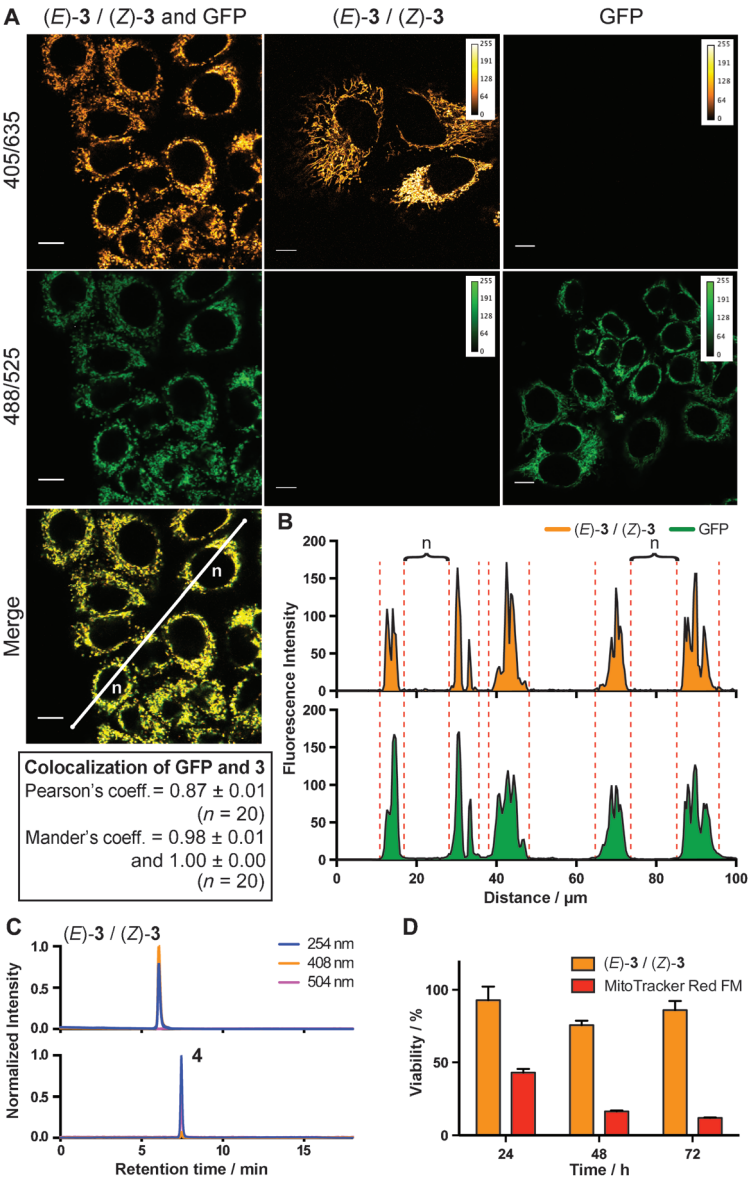

Figure 2. A) Confocal images of mito-GFP cells (right), HeLa cells stained with (*E*)-**3**/(*Z*)-**3** (middle), and mito-GFP cells stained with (*E*)-**3**/(*Z*)-**3** (left). Compound (*E*)-**3**/(*Z*)-**3** was observed at 405/635 nm while GFP was observed at 488/525 nm. All images were kept at the same contrast/brightness, and bleed-through between channels was not detected. Scale bar: 10 µm. B) Line plot of the fluorescence intensity across multiple cells showing high colocalization and signal-to-noise ratios for both GFP and (*E*)-**3**/(*Z*)-**3**. In the colocalization plot in the bottom left of panel A, the nuclear regions in adjacent cells are designated with "n". Pearson's colocalization coefficient: 0.87 ± 0.01; Manders' overlap coefficients: 0.98 ± 0.01 and 1.00 ± 0.00. C) HPLC chromatogram of (*E*)-**3**/(*Z*)-**3** (1 mM solution in water) after ten days under ambient light (top chromatogram) and HPLC chromatogram of **4** (bottom chromatogram). No decomposition products or the photoproduct of (*E*)-**3**/(*Z*)-**3** were detected. D) The cell viability was determined using HeLa cells in the presence of (*E*)-**3**/(*Z*)-**3** (5 µM) or MitoTracker Red FM (1 µM).

Compound (*E*)-**3**/(*Z*)-**3** is fluorescent with a large Stokes shift (135 nm). Photoproduct **4** is red-shifted in both absorbance and emission by approximately 100 nm while a large Stokes shift of 108 nm is retained (Figure 1C). Live-cell imaging studies of (*E*)-**3**/(*Z*)-**3** were performed with HeLa cells, and specific sub-cellular localization was observed, consistent with mitochondrial uptake. An engineered HeLa cell line that expresses GFP-labeled proteins specifically localized to the outer mitochondrial membrane (mito-GFP cell line, Figure S3), as introduced in one of our previous studies,[5b] was used as a control to confirm the mitochondrial localization of (*E*)-**3**/(*Z*)-**3** in this report. The localization statistics were also compared to those of a commonly used and commercially available MitoTracker dye (Figure S4).[8] Our control cell line consisted of a population of HeLa cells expressing a GFP fusion protein localized specifically to the outer mitochondrial membrane (mito-GFP cell line) in addition to a population of non-GFP-expressing HeLa cells, which served as an internal control for compound localization in the absence of the GFP signal. The two channels 405/635 and 488/525 were used to detect (*E*)-**3**/(*Z*)-**3** and GFP, respectively, with no bleed-through observed. All images were recorded at the same brightness and contrast settings. Incubating mito-GFP cells with (*E*)-**3**/(*Z*)-**3** allowed for colocalization to be assessed (Figure 2A and Figure S3). Colocalization statistics calculated over multiple frames for a total of 80 cells showed significant overlap (Pearson's coefficient: 0.81 ± 0.02; Manders' coefficients: 0.98 ± 0.01 and 1.00 ± 0.00; Spearman correlation: 0.88 ± 0.02). High Manders' coefficients point to near exclusive mitochondrial localization of (*E*)-**3**/(*Z*)-**3** in GFP-positive cells. Variations in intensity between localized (*E*)-**3**/(*Z*)-**3** and GFP resulted in a slightly lower Pearson's coefficient. This small deviation may be attributed to the difference between internal mitochondrial localization of (*E*)-**3**/(*Z*)-**3** versus external mitochondrial membrane localization of GFP. Intensity profiles across multiple cells are shown in Figure 2B. Additional colocalization studies were carried out using commercially available Mitotracker Red,[8] and similar results were observed when comparing the colocalization with GFP-labeled mitochondria (Figure S4). High signal-to-noise ratios were observed in the intensity line plots for both GFP and (*E*)-**3**/(*Z*)-**3** (Figure 2B). The stability of a 1 mM aqueous solution of (*E*)-**3**/(*Z*)-**3** was assessed under ambient light conditions at 25 °C for ten days. HPLC analysis of the resulting solution revealed no evidence for decomposition or photoconversion compared to a standard sample of photoproduct **4** (Figure 2C). Cytotoxicity studies on HeLa cells over 24, 48, and 72 hours confirmed that (*E*)-**3**/(*Z*)-**3** had very low cytotoxicity. For comparison, MitoTracker Red FM, one of the most commonly used mitochondrial imaging probes, showed significant cytotoxicity over the same time course at a five-fold lower concentration (Figure 2D).

By combining the observed photoreaction (Figure 1A) with the ability to selectively label mitochondria for live-cell imaging (Figure 2A), intracellular photoactivation of (*E*)-**3**/(*Z*)-**3** was attempted. As the absorbance and emission spectra of **4** are red-shifted by approximately 100 nm compared to those of (*E*)-**3**/(*Z*)-**3**, the individual species can be selectively excited. Alternating use of the two channels (i.e., 444/525 for (*E*)-**3**/(*Z*)-**3** and 488/632 for **4**) resulted in the photoconversion of (*E*)-**3**/(*Z*)-**3** into **4** in live cells. A significant increase in the fluorescence intensity of **4** was achieved after 30 seconds, using 200 total scans (Figure 3A,B). To further investigate the spatial selectivity, a targeted 405 nm laser (CrystaLaser, DL405-050-O) was used to target smaller areas of the cells. Confocal images were captured using a 488 nm excitation laser and a 632 nm emission filter. Immediately after the first activation, a bright signal was detected at the targeted region. The tubular morphology of the mitochondria was observed, and the remaining portions of the mitochondria remained dim for an additional ten seconds using the 488 nm excitation laser (Figure 3C).

Finally, we wanted to show that individual cells can be photoactivated in extremely crowded confluent cellular environments. A normalized intensity plot for the sequential photoactivation of two adjacent cells is shown in Figure 3C. A standard 405 nm laser commonly used for photobleaching

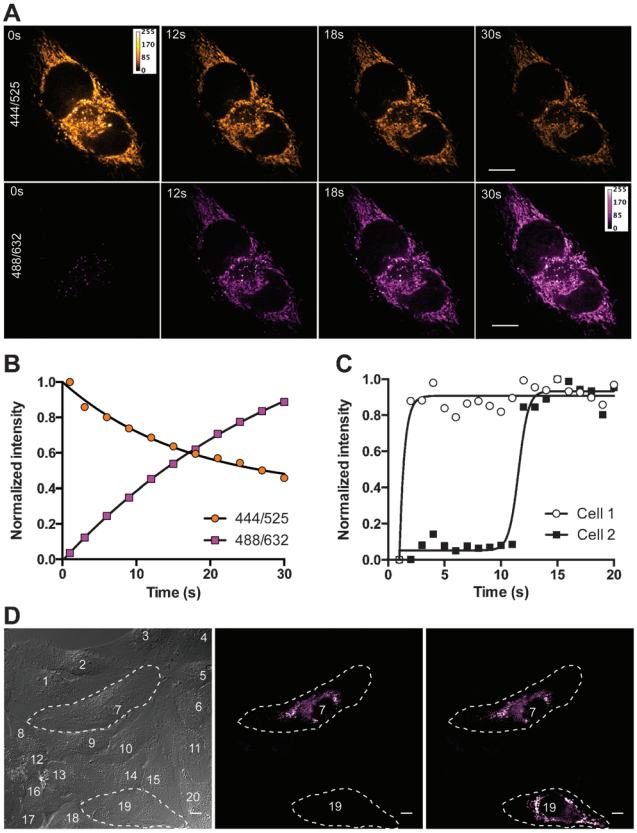

Figure 3. A) Confocal microscopy images of HeLa cells stained with (*E*)-**3**/(*Z*)-**3**, observed at 444/525 nm and 488/632 nm over 30 s with 200 alternating 150 ms pulses. B) Average intensity of the 444/525 and 488/632 channels after 200 alternating pulses. The data from each of the two channels were fitted to a one-phase exponential curve, and the obtained rate constants and half-lives were 0.060 s^{-1} and 11.61 s for the 444/525 channel and 0.030 s^{-1} and 23.05 s for the 488/632 channel. C) Normalized intensity plot for the sequential photoactivation of two cells. D) Selective sequential photoactivation of two cells (7 and 19) among a field of view containing 20 confluent cells. Each cell was activated by fifty 20 s pulses of a normal 405 nm FRAP laser. Dashed lines indicate cell boundaries. Scale bar: 10 μm.

experiments was used for sequential photoactivation with excellent spatial control over individual cells in crowded environments (Figure 3D). Using 50 pulses with a length of 20 s, the mitochondrial probe **3** was photoconverted into **4**. Two individual cells out of 20 cells were sequentially photoactivated (cell 7 and cell 19, Figure 3D).

In conclusion, we have developed a photoactivatable probe that is based on a 6π electrocyclization/oxidation mechanism. The probe is water-soluble, cell-permeable, non-cytotoxic, and can selectively stain mitochondria. This photoactivation strategy should be broadly applicable to many dye classes, and further studies are underway to develop new cellular imaging tools.

Keywords: electrocyclization · fluorescent probes · imaging agents · photochemistry

How to cite: *Angew. Chem. Int. Ed.* **2015**, *54*, 6442–6446
Angew. Chem. **2015**, *127*, 6542–6546

[1] a) K. A. Lukyanov, D. M. Chudakov, S. Lukyanov, V. V. Verkhusha, *Nat. Rev. Mol. Cell Biol.* **2005**, *6*, 885–891; b) A. Welman, A. Serrels, V. G. Brunton, M. Ditzel, M. C. Frame, *J. Biol. Chem.* **2010**, *285*, 11607–11616; c) V. V. Verkhusha, A. Sorkin, *Chem. Biol.* **2005**, *12*, 279–285; d) G. H. Patterson, J. Lippincott-Schwartz, *Methods* **2004**, *32*, 445–450; e) D. M. Shcherbakova, V. V. Verkhusha, *Curr. Opin. Chem. Biol.* **2014**, *20*, 60–68; f) V. Adam, R. Berardozzi, M. Byrdin, D. Bourgeois, *Curr. Opin. Chem. Biol.* **2014**, *20*, 92–102.

[2] a) E. Lacivita, M. Leopoldo, F. Berardi, N. A. Colabufo, R. Perrone, *Curr. Med. Chem.* **2012**, *19*, 4731–4741; b) M. Fernández-Suárez, A. Y. Ting, *Nat. Rev. Mol. Cell Biol.* **2008**, *9*, 929–943.

[3] a) R. Ando, H. Hama, M. Yamamoto-Hino, H. Mizuno, A. Miyawaki, *Proc. Natl. Acad. Sci. USA* **2002**, *99*, 12651–12656; b) M. Tomura, N. Yoshida, J. Tanaka, S. Karasawa, Y. Miwa, A. Miyawaki, O. Kanagawa, *Proc. Natl. Acad. Sci. USA* **2008**, *105*, 10871–10876; c) I. Hayashi, H. Mizuno, K. I. Tong, T. Furuta, F. Tanaka, M. Yoshimura, A. Miyawaki, M. Ikura, *J. Mol. Biol.* **2007**, *372*, 918–926; d) P. S. Dittrich, S. P. Schäfer, P. Schwille, *Biophys. J.* **2005**, *89*, 3446–3455.

[4] a) S. Y. Cho, Y. K. Song, J. G. Kim, S. Y. Oh, C. M. Chung, *Tetrahedron Lett.* **2009**, *50*, 4769–4772; b) N. Gagey, P. Neveu, C. Benbrahim, B. Goetz, I. Aujard, J. B. Baudin, L. Jullien, *J. Am. Chem. Soc.* **2007**, *129*, 9986–9998.

[5] a) T. Faal, P. T. Wong, S. Tang, A. Coulter, Y. Chen, C. H. Tu, J. R. Baker, S. K. Choi, M. A. Inlay, *Mol. BioSyst.* **2015**, *11*, 783–790; b) E. R. Ballister, C. Aonbangkhen, A. M. Mayo, M. A. Lampson, D. M. Chenoweth, *Nat. Commun.* **2014**, *5*, 5475; c) T. Kobayashi, T. Komatsu, M. Kamiya, C. Campos, M. Gonzalez-Gaitan, T. Terai, K. Hanaoka, T. Nagano, Y. Urano, *J. Am. Chem. Soc.* **2012**, *134*, 11153–11160.

[6] S. J. Lord, N. R. Conley, H. L. D. Lee, R. Samuel, N. Liu, R. J. Twieg, W. E. Moerner, *J. Am. Chem. Soc.* **2008**, *130*, 9204–9205.

[7] a) R. K. V. Lim, Q. Lin, *Acc. Chem. Res.* **2011**, *44*, 828–839; b) Z. Yu, L. Y. Ho, Q. Lin, *J. Am. Chem. Soc.* **2011**, *133*, 11912–11915; c) P. An, Z. Yu, Q. Lin, *Org. Lett.* **2013**, *15*, 5496–5499.

[8] I. Johnson, M. T. Z. Spence, *Molecular probes handbook*: *a guide to fluorescent probes and labeling technologies*, *11th ed.*, Life Technologies Corp., **2010**.

[9] R. A. Rarig, M. N. Tran, D. M. Chenoweth, *J. Am. Chem. Soc.* **2013**, *135*, 9213–9219.

[10] J. Sandström, *Dynamic NMR spectroscopy*, Academic Press, London, New York, **1982**.

[11] a) E. V. Anslyn, D. A. Dougherty, *Modern physical organic chemistry*, University Science Books, Sausalito, **2006**; b) I. Fleming, *Molecular Orbitals and Organic Chemical Reactions*, Wiley, Chichester, **2009**.

[12] Gaussian 09 (Revision B.01 ed.), M. J. T. Frisch et al., Wallingford, CT, **2010**.

Received: March 14, 2015
Published online: May 7, 2015

